Talanta 240 (2022) 123171

Contents lists available at ScienceDirect

Talanta

journal homepage: www.elsevier.com/locate/talanta

# A $FeS_2$NPs-Luminol-$MnO_2$NSs system based on chemiluminescence resonance energy transfer platform for sensing glutathione

Xiaomin Liu [a], Qian Fan [b], Xiaoxu Zhang [a], Ming Li [c], Yanfu Huan [a], Pinyi Ma [a], Daqian Song [a], Qiang Fei [a,*]

[a] College of Chemistry, Jilin University, Changchun, 130023, China
[b] Changchun Polytechnic, Changchun, 130033, China
[c] The National Institute of Metrology, Beijing, 100029, China

ARTICLE INFO

*Keywords:*
Ferrous disulfide nanoparticles ($FeS_2$NPs)
Luminol
Chemiluminescence resonance energy transfer (CRET)
$MnO_2$ nanosheets ($MnO_2$NSs)
Glutathione (GSH)

ABSTRACT

In this work, ferrous disulfide nanoparticles ($FeS_2$NPs) with oxidase properties were synthesized, and a $FeS_2$NPs-Luminol-$MnO_2$ nanosheets ($MnO_2$NSs) chemiluminescence resonance energy transfer (CRET) system was successfully established. Because of reaction with $MnO_2$NSs, glutathione (GSH) can inhibit CRET between Luminol and $MnO_2$NSs and recover the luminescence intensity of $FeS_2$NPs-Luminol. Consequently, we developed a GSH sensor based on this chemiluminescence resonance energy transfer (CRET) system. Under optimal conditions, the $FeS_2$NPs-Luminol-$MnO_2$NSs sensing system showed very sensitive response to GSH in the range of 1 μM–500 μM. The limit of detection of GSH reached as low as 0.15 μM. Finally, the sensor was successfully used for the detection of GSH in serum.

## 1. Introduction

Reactive Sulfur Species (RSS) is a general term of sulfur-containing biomolecules in organisms and one of the endogenous active Species in organisms [1], including hydrogen sulfide, glutathione, cysteine, and the like, among which glutathione is the most common nonprotein mercaptan in the cell [2]. Glutathione (GSH) is a tripeptide containing sulfhydryl groups that combines glutamate, cysteine and glycine [3]. It has antioxidant and integrative detoxification effects [4]. As an important intracellular regulatory metabolite, the level changes of GSH have been associated with a variety of diseases, such as leukocyte loss, psoriasis, liver injury, Parkinson's disease, and more [2]. Therefore, there is considerable interest in developing rapid and accurate detection systems for use in the clinic.

Many methods for detecting GSH have been spotted in recent years, such as fluorescent spectrometry [5,6], UV–Visible absorption spectrum [7], mass spectrometry [8] and other. However, these methods still have some disadvantages, such as background interference of excitation light source, expensive instrument, complicated operation and more. Chemiluminescence can just avoid these deficiencies and become an excellent detection method for GSH. Therefore, we developed a system for GSH detection based on chemiluminescence resonance energy transfer (CRET).

Chemiluminescence is the light phenomenon derived from the chemical reaction [9,10]. Compared with fluorescence, chemiluminescence is not influenced by autofluorescence and light scattering, so it has been extensively employed in various fields [11–13]. As a typical chemiluminescence system, Luminol-$H_2O_2$ has been widely used in criminal investigation [14] and detection of various biomolecules [15,16] and metal ions [17,18]. However, $H_2O_2$ easy to self-decomposition, is unfavorable to acquire highly stable emission [9,19,20]. To avoid the problems, ferrous disulfide nanoparticles ($FeS_2$NPs) with oxidase activity were synthesized and $FeS_2$NPs–Luminol-$O_2$ chemiluminescence system was established. The system has strong stability and high luminescence intensity.

Chemiluminescence resonance energy transfer (CRET) is a non-radiative dipole-dipole energy transfer process that transfers the excited state energy of the donor molecule generated by chemical reaction to the recipient molecule [21], which is a very attractive optical analysis method. These days, the introduction of quantum dots [22], graphene [23], amorphous carbon nanoparticles [24] and 2-D transition metal disulfide [21] compound nanosheets as energy receptors have made significant progress in CRET system. Most of the two-dimensional transition metal oxide nanomaterials (TMONs) have absorption

* Corresponding author.
*E-mail address:* feiqiang@jlu.edu.cn (Q. Fei).

https://doi.org/10.1016/j.talanta.2021.123171
Received 12 November 2021; Received in revised form 20 December 2021; Accepted 21 December 2021
Available online 23 December 2021
0039-9140/© 2021 Elsevier B.V. All rights reserved.

properties due to strong d-d transitions [25]. Therefore, it has been reported that $MnO_2$NSs is commonly applied for fluorescence resonance energy transfer (FRET) detection [26–28], but rarely for CRET.

In this work, a $FeS_2$NPs-Luminol-$MnO_2$NSs chemiluminescence resonance energy transfer (CRET) system has been successfully established, in which luminol was the chemiluminescence resonance energy donor and $MnO_2$NSs was the receptor. Because of reaction with $MnO_2$NSs, GSH can inhibit CRET between Luminol and $MnO_2$NSs, and recover the luminescence intensity of $FeS_2$NPs-Luminol. Consequently, we developed a GSH sensor based on chemiluminescence resonance energy transfer (CRET) platform.

## 2. Experimental section

### 2.1. Chemicals and materials

#### 2.1.1. Reagents

Luminol was obtained from Sun Chemical Technology Co., Ltd. 3-morpholinopropanesulfonic acid (MOPS) was provided by Energy Chemical, $KMnO_4$ by Sinopharm Chemical Reagent Co., Ltd. (China). $MgCl_2$ was purchased from Tianjin Guangfu Technology Development Co., Ltd, and NaCl from Tianjin Tian tai Chemical Co., Ltd. Sodium Acetate, Anhydrous Ferric Chloride ($FeCl_3$), $CuSO_4$, NaOH, Glutathione (GSH), Cysteine (Cys), Glycine (Gly), Leucine (Leu), Serine (Ser), Valine (Val), Tryptophan (Try) and Threonine (Thr) were supplied by Beijing Chemical Works. All chemicals were of analytical grade and had not been further purification.

A 10 mM stock solution of luminol was prepared by dissolving luminol in 0.1 M NaOH solution for a week in a dark room and stored at room temperature.

#### 2.1.2. Instruments

The RFL-1 ultra-weak luminescence analyzer (Xi'an Remex Analysis Instrument Co., Ltd, China) was used to record the whole process of the experiment. Luminol's emission wavelength was acquired on the F-2700 spectrofluorometer (Hitachi, Japan) that turned off the Xe lamp. The absorption spectra of $FeS_2$NPs and $MnO_2$NSs were captured on the UV-3100 UV–VISNIR spectrofluorometer (Shimadzu, Japan). Morphologies of $FeS_2$NPs and $MnO_2$NSs were investigated by using a JEM2100F transmission electron microscopy (TEM, JEOL. Co., Ltd, Japan). Raman spectra were obtained with a Renishaw inVia Raman microspectrometer. Fourier transform infrared (FT-IR) spectra were obtained as KBr disks with the Avatar 360 (Nicolet, USA) spectrometer. X-ray diffraction (XRD) patterns were performed on a 6100 Lab diffractometer (Shimadzu) with a Cu Kα radiation.

### 2.2. Synthesis of $FeS_2$NPs and $MnO_2$NSs

$FeS_2$NPs was synthesized by solvothermal method referring to the previous method [29]. Briefly, 0.49 g $FeCl_3$ was dissolved in 40 mL ethylene glycol and vigorously stirred for 30 min at room temperature. After that, 3.6 g sodium acetate and 5 g cysteine were introduced to the mixture and stirring for another 30 min. The solution was put into a 20 mL Teflon autoclave. After 4 h of reaction at 200 °C followed by cooling to room temperature, the target product was obtained by vacuum filtration and rinsed alternately with ethanol and deionized water. Dry the washed solids overnight in the drying oven. Solid samples were dispersed with deionized water for experimental use.

$MnO_2$NSs was prepared according to the previous method [30]. Firstly, 0.21 g 3-Moroline propionic acid (MOPS) and 0.0158 g $KMnO_4$ were mixed in 10 mL deionized water. Then the mixture was subjected to ultrasonic treatment at room temperature for 30 min. The dark brown flocculent was centrifuged at 10,000 rpm for another 10 min, and finally washed with water. The flocculent was dispersed in 10 mL deionized water for the following usage. The concentration $MnO_2$NSs was 14.69 mM, calculated with the molar extinction coefficient of $9.6\times10^3$ $M^{-1}$ $cm^{-1}$ (380 nm) [30].

### 2.3. Analytical procedure

For the CL determination of GSH, 100 μL $MnO_2$NSs (2 mM) and 100 μL GSH with different concentrations were, respectively, mixed for incubation in test tube. After 15 min, 100 μL $FeS_2$NPs (2 mg/mL) was introduced to the mixture and diluted with deionized water to 500 μL. The prepared reagent was transferred to a 5 mL beaker and placed in the dark chamber of the detector. Finally, 500 μL Luminol (0.1 mM) was injected with an injection pump and the luminescence intensity of the system was recorded.

### 2.4. Sensing detection of serum samples

To verify the practicability of this sensing system, we used this system to detect GSH in serum. The GSH of the serum sample was tested using the above-depicted procedure, except that the 100 μL GSH solution was replaced with 100 μL serum.

## 3. Results and discussion

### 3.1. Characterization of $FeS_2$NPs and $MnO_2$NSs

The morphology of the $FeS_2$NPs and $MnO_2$NSs was observed by TEM. As shown in Fig. 1 (A and B), the $FeS_2$NPs exhibit a morphology of spheres and a rough surface with the diameter of 1–2 μm, due to the oriented assembly of amounts of $FeS_2$NPs. As shown in Fig. 1 (C and D), the prepared brown $MnO_2$ suspension present obvious morphology of nanosheet with the diameter of 100–150 nm.

XRD analysis demonstrate in Fig. 2 (A) that the diffraction peaks (black) of $FeS_2$NPs can be well assigned to that of the $FeS_2$ at $2\theta = 28.5^\circ$ (111), 33.1° (200), 37.1° (210), 40.8° (211), 47.4° (220) and 56.3° (311) and suggest that the $FeS_2$ core was successfully synthesized. The significant XRD peaks (red) can be well assigned to the $MnO_2$ with a hexagonal birnessite structure. The diffraction signals at $2\theta = 12.3^\circ$, 18.7°, 36.8°, 54.9° and 65.7° can be attributed to the (002), (101), (006), (301) and (119), respectively.

The FT-IR spectra in Fig. 2 (B) indicate that the synthesized $FeS_2$NPs exhibit three characteristic absorption peaks at 418 $cm^{-1}$, 1058 $cm^{-1}$, and 1400 $cm^{-1}$, consistent with standard infrared spectrogram of $FeS_2$ at 407 $cm^{-1}$, 1065 $cm^{-1}$ and 1400 $cm^{-1}$418 $cm^{-1}$ and 1058 $cm^{-1}$ belong to stretching vibration of $Fe^{2+}$-$[S_2]^{2-}$ and S–S, respectively [31]. Because the prepared $FeS_2$NPs are not pure $FeS_2$, the peaks at 418 $cm^{-1}$ and 1058 $cm^{-1}$ shift to higher wavenumber and lower wavenumber, respectively. Besides, the peaks 1633 $cm^{-1}$ and 3448 $cm^{-1}$ are caused by the deformation and stretching vibration of hydroxyl groups. According to the above analysis, it indicates that $FeS_2$NPs have been successfully synthesized. It is worth noting that 613 $cm^{-1}$ should be attributed to the Fe–O bond in $Fe_3O_4$, showing that the prepared $FeS_2$NPs have a small amount of $Fe_3O_4$ [29]. The prepared $MnO_2$NSs exhibit FT-IR peaks at 556 $cm^{-1}$, 1636 $cm^{-1}$, and 3431 $cm^{-1}$, which can be assigned correspondingly to the Mn–O stretching, O–H bending, and O–H stretching, consistent with reported results [32].

In addition, $MnO_2$NSs have been characterized by UV–vis spectroscopy and Raman spectrum. $MnO_2$NSs display an extensive absorption band within 300–800 nm, and the maximum absorption peak at around 380 nm can be attributed to the d-d transition of $Mn^{4+}$ ion (Fig. 2 (C)) [32]. The Raman shifts at 574.6 $cm^{-1}$ and 649.2 $cm^{-1}$ can be contributed to the Mn–O vibration (Fig. 2 (D)), which is similar to that of previous report [33].

### 3.2. GSH detection principle

When the emission spectrum of the chemiluminescence substrate (energy donor) and the absorption spectrum of the energy receptor

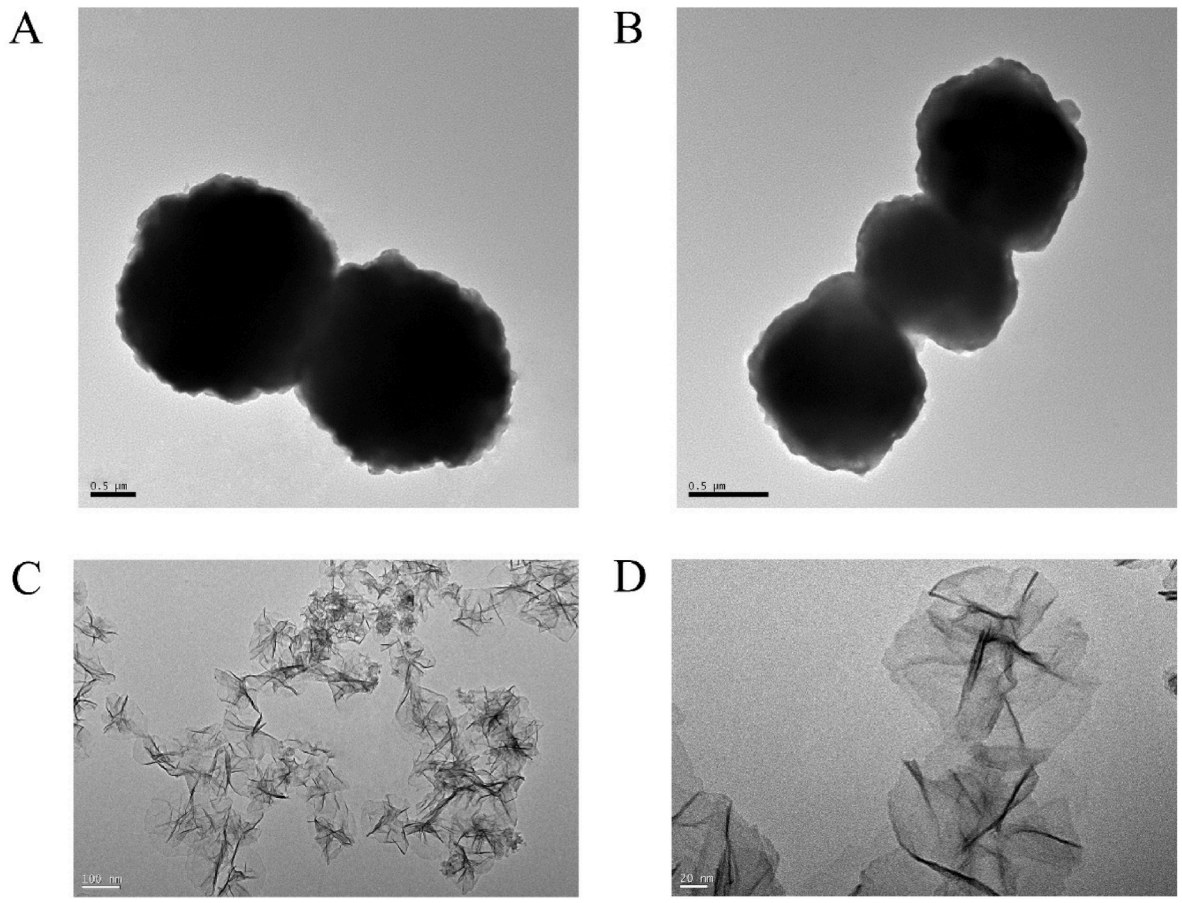


**Fig. 1.** Exhibits the TEM of the as-synthesized $FeS_2$NPs (A and B) and $MnO_2$NSs (C and D).

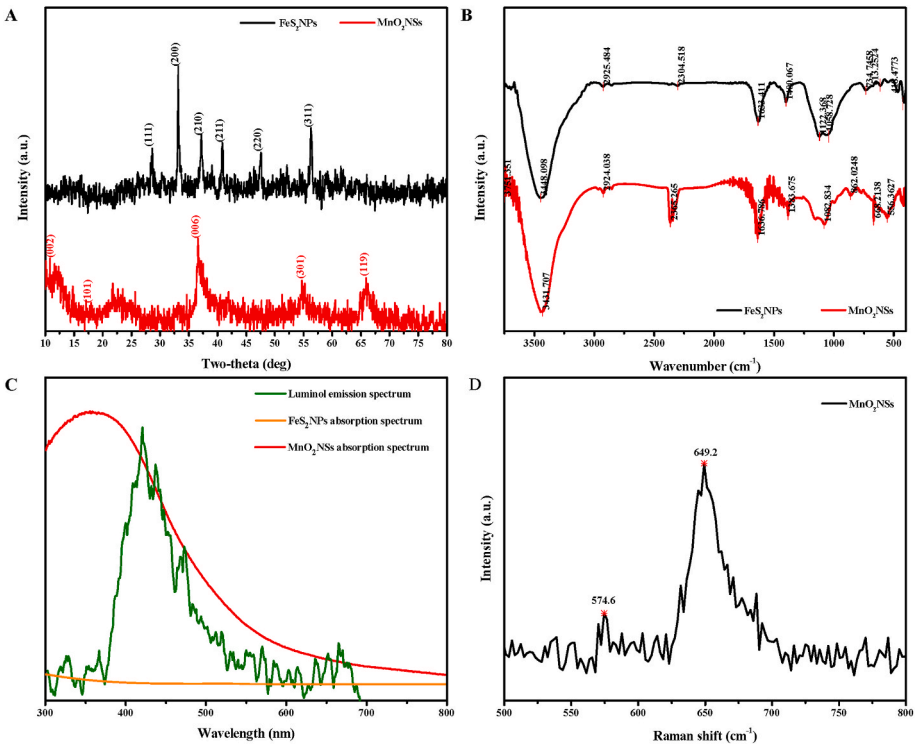


**Fig. 2.** (A) The XRD of the as-synthesized $FeS_2$NPs and $MnO_2$NSs. **(B)** The FT-IR spectra of $FeS_2$NPs and $MnO_2$NSs. **(C)** UV–vis spectra of $MnO_2$NSs and $FeS_2$NPs, and chemiluminescence spectrum of luminol. **(D)** Raman spectrum of $MnO_2$NSs.

effectively overlap, and the space distance between the energy donor and the energy receptor of the chemical reaction is relatively close, the chemiluminescence resonance energy transfer (CRET) can be generated. As can be seen from Fig. 2 (C), luminol has an emission band within 380 nm–550 nm in this study, while $MnO_2$NSs have an extensive absorption band in the wavelength range of 300 nm–800 nm. However, there was no obvious absorption signal of the $FeS_2$NPs in the range of 300 nm–800 nm, indicating that there was no possibility of CRET between $FeS_2$NPs and luminol. In addition, $FeS_2$NPs have strong adsorption [34,35], which can ensure that the distance between luminol and $MnO_2$NSs is close enough. $MnO_2$NSs and GSH can undergo REDOX reaction, as can be seen in Fig. 3 (C) that the absorbance of $MnO_2$NSs decreased significantly in the presence of GSH. $MnO_2$NSs was reduced to $Mn^{2+}$ (Fig. 3 (D)) and CRET between Luminol and $MnO_2$NSs was destroyed. Therefore, we designed a GSH sensor based on CRET between $FeS_2$NPs-Luminol and $MnO_2$NSs, and selective REDOX reactions between $MnO_2$NSs and GSH (Scheme 1).

Some experiments results are shown in Fig. 3 (A). When only $FeS_2$NPs and Luminol presented in the system, Luminol was oxidized by dissolved oxygen under the catalysis of $FeS_2$NPs and had a strong emission. When the system contained $FeS_2$NPs, Luminol and $MnO_2$NSs, the luminescent intensity of the system was visibly quenched due to the CRET interaction between $FeS_2$NPs-Luminol and $MnO_2$NSs. However, when GSH was introduced to the $FeS_2$NPs-Luminol-$MnO_2$NSs system, the luminescence intensity was recovered. That's because the CRET between Luminol and $MnO_2$NSs was destroyed by GSH. With the increase of GSH concentration, the luminescence intensity increased with linear.

There were also more evidences to support this mechanism. As can be seen from the Fig. 2 (C), its emission wavelength was at 425 nm, which indicated that the 3-aminophthalate anions (3-APA*) was still luminescent. Meantime, it can be seen from the Fig. 3 (A) that $FeS_2$NPs greatly enhanced the emission of Luminol. To verify the role of dissolved oxygen in the system, Fig. 3 (B) shows the luminescence intensity under different solution saturated with air, oxygen and nitrogen, respectively, containing $FeS_2$NPs and Luminol. It can be seen that the intensity of the solution saturated with oxygen was higher than that of the saturated with air, while that of the solution saturated with nitrogen decreased significantly. Studies have shown that oxygen can be adsorbed on the surface of $FeS_2$NPs [36,37]. Therefore, through this part of the work, not only had the role of oxygen been affirmed, but the oxidase properties of $FeS_2$NPs had been verified.

### 3.3. Optimization of the sensing conditions

To obtain higher sensitivity, the parameters of the sensor were optimized for the detection of GSH. We first explored the influence of $FeS_2$NPs concentration, as shown in Fig. 4 (A). As $FeS_2$NPs concentration increased, the signal strength increased, then decreased, and finally a platform appeared. when the concentration of $FeS_2$NPs in the system was 0.2 mg/mL, the chemiluminescence intensity of the system was the maximum. Fig. 4 (B) shows the influence of $MnO_2$NSs concentration on luminous signal intensity. It can be concluded that the concentration of $MnO_2$NSs was inversely proportional to the signal intensity. When its concentration reached 0.2 mM, the signal intensity changed slightly. Therefore, 0.2 mM $MnO_2$NSs was selected in the experiment. As shown

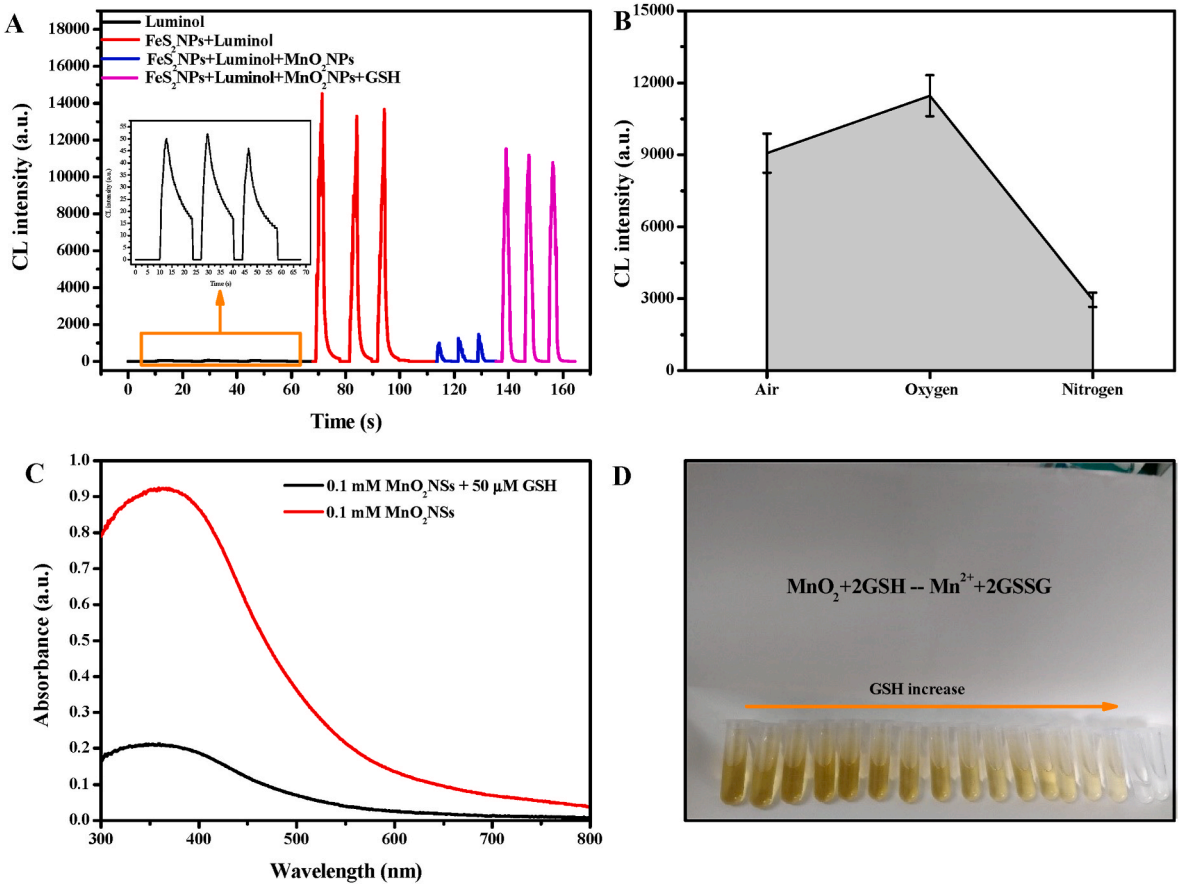


**Fig. 3.** (A) Effects of $FeS_2$NPs, $MnO_2$NSs and GSH on the system (0.01 mM luminol; 0.2 mg/mL $FeS_2$NPs; 0.2 mM $MnO_2$NSs; 50 μM GSH). **(B)** Effects of air, oxygen and nitrogen on the system (0.01 mM luminol; 0.2 mg/mL $FeS_2$NPs). **(C)** Absorption spectra of $MnO_2$ NSs in the absence and presence of GSH (0.1 mM $MnO_2$ NSs; 50 μM GSH). **(D)** Interaction between GSH and $MnO_2$NSs (the concentration of GSH: 0, 0.1 μM, 0.5 μM, 1 μM, 5 μM, 10 μM, 20 μM, 30 μM, 40 μM, 50 μM, 60 μM, 70 μM, 80 μM, 90 μM, 100 μM, 500 μM, 1000 μM; $MnO_2$NSs: 0.1 mM).

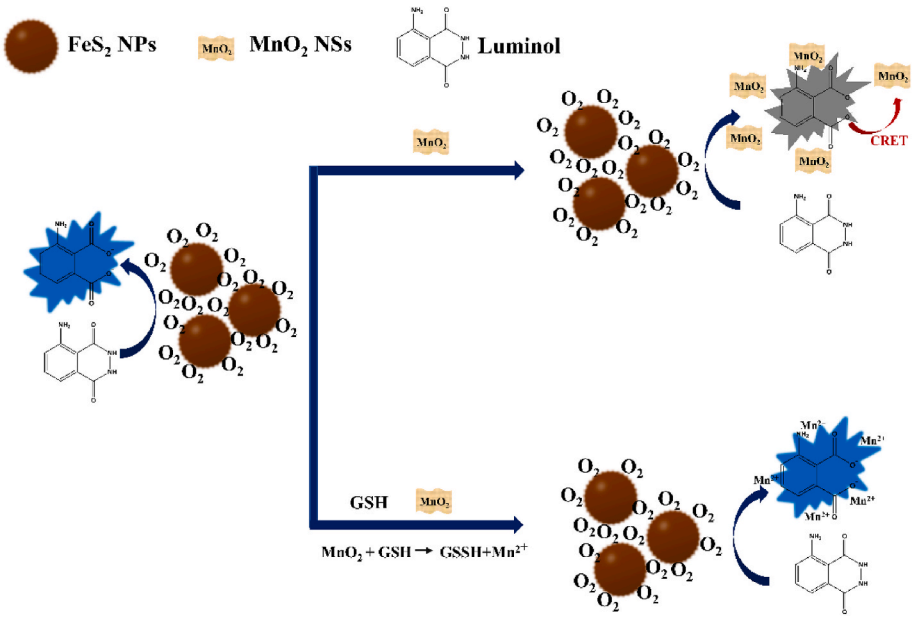


**Scheme 1.** Principle of sensor of GSH based on CRET.

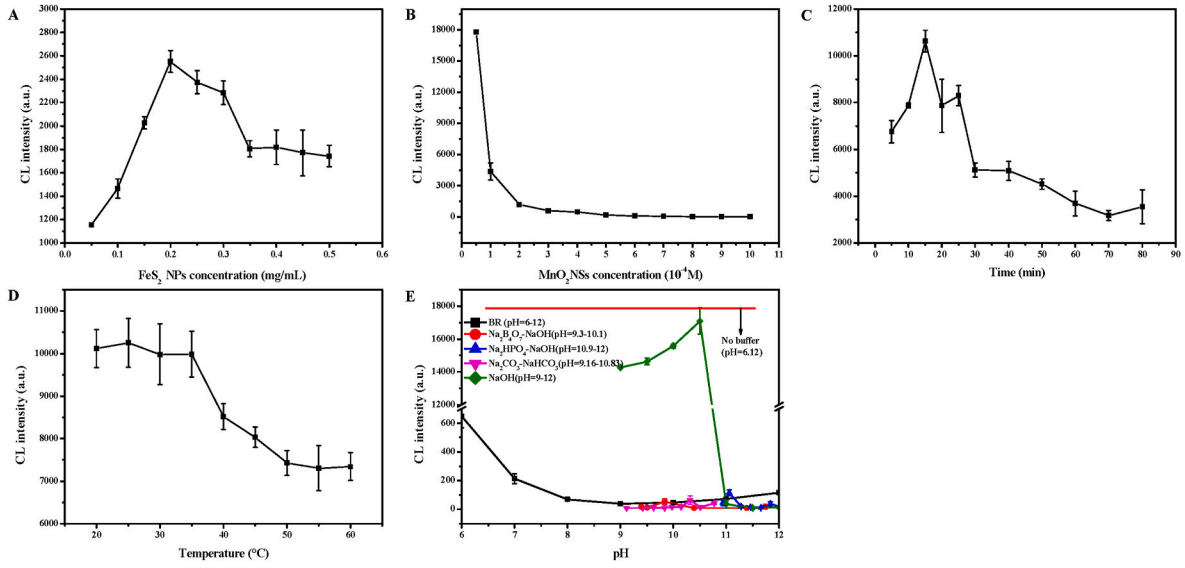


**Fig. 4.** Influence of $FeS_2$NPs concentration **(A)**, $MnO_2$NSs concentration **(B)**, incubation times **(C)**, incubation temperature **(D)** and buffer solution (BR, $Na_2B_4O_7$–NaOH, $Na_2HPO_4$–NaOH, $Na_2CO_3$–$NaHCO_3$ and NaOH) **(E)**.

in Fig. 4 (C), we found that the chemiluminescence intensity first increased and then decreased with the increase of incubation time. When the incubation time was 15 min, the signal value can reach the maximum. We also explored the influence of incubation temperature on the experiment. As shown in Fig. 4 (D), the chemiluminescence intensity was basically stable when incubation temperature was between 20°C and 35 °C. When the temperature was higher than 35 °C, the luminescence intensity began to decrease, which might be because the reaction system was broken by high temperature. Therefore, incubation at room temperature is sufficient to meet experimental requirements. Finally, the effects of Britton-Robison (BR), $Na_2B_4O_7$–NaOH, $Na_2HPO_4$–NaOH and $Na_2CO_3$–$NaHCO_3$ buffer on the reaction systems in their respective buffer ranges were investigated. In Fig. 4 (E), the group with no buffer (red line) had a much larger signal than the group with buffer. The chemiluminescence intensity of BR buffer decreased with pH increase. Moreover, the BR buffer at pH = 6 was much smaller than the signal in the unbuffered group (pH = 6.12). We were curious about this phenomenon, so we added NaOH with different pH to this system. With the increase of pH, the signal increased first, and when pH = 10.5, the signal was comparable to that of the group without buffer. But when the pH was above 10.5, the signal dropped sharply. Therefore, we suspected that high concentration of ions inhibited chemiluminescence signals, and buffer solution was not used in subsequent experiments.

### 3.4. Detection of GSH

To demonstrate the applicability of the developed sensor for GSH detection, we tested the response of the assay to different concentrations of GSH under optimal conditions. As shown in Fig. 5 (A), the concentration of GSH was directly proportional to the signal intensity. Moreover, it can be seen that a linear relationship was obtained in the range of 1–500 μM (Fig. 5 (B)) and the limit of detection (LOD) of GSH was

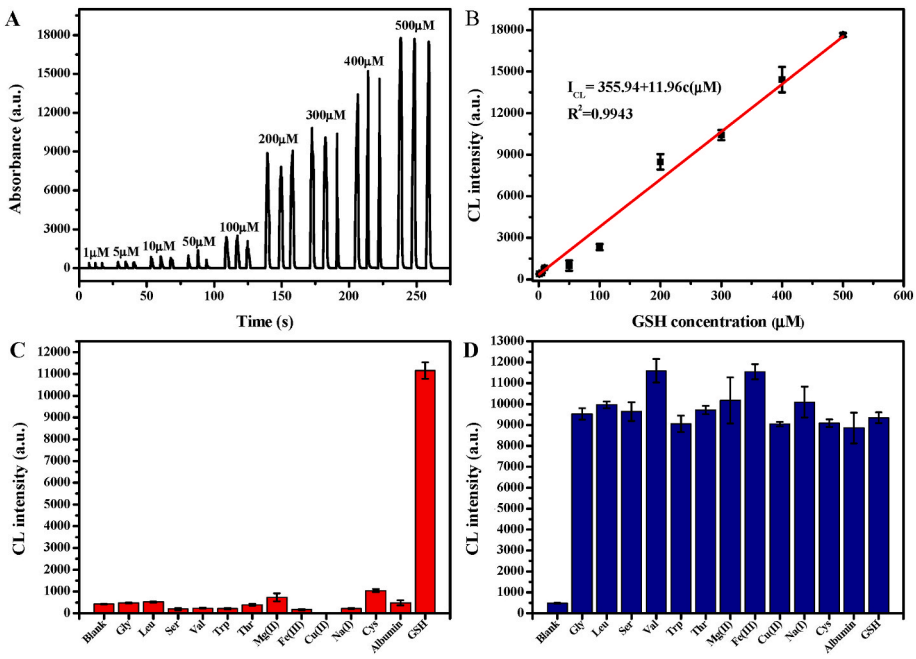


**Fig. 5.** (A) The value of the chemiluminescence signal varied with the GSH concentration from 1 to 500 μM. **(B)** Calibration curve of $FeS_2$NPs-Luminol-$MnO_2$NSs system for GSH detection. The selectivity **(C)** and anti-interference **(D)** of this assay.

0.15 μM (LOD = 3σ/b; σ: standard deviation of blank value, σ = 0.58; b: slope of the standard curve, b = 11.96). The results show that the method has high sensitivity, low detection limit and wide linear range.

### 3.5. Selectivity and anti-interference of this system

To evaluate the selectivity of this assay, we investigated its response to some 5 mM electrolytes and amino acids, 75 μM (5 g/L) albumin as well as 50 μM cysteine and glutathione (GSH). As shown in Fig. 5 (C), the luminescence intensity of GSH added was significantly higher than that of others with relatively higher concentration and cysteine with same concentration. This result suggests that the method is more selective for GSH than other non-target samples.

To estimate the anti-interference of this system, we explored its response to some electrolytes and amino acids. In this section, the concentration of $Mg^{2+}$, $Fe^{3+}$, $Cu^{2+}$, $Na^{+}$, cysteine and albumin were 100 μM, 2.5 μM, 2.5 μM, 14 mM, 10 μM and 75 μM (the concentration of these near to the physiologic concentration), respectively, and the rest were as 50 μM (Fig. 5 (D), the luminescence intensity had no significant difference. This result suggests that this system has better anti-interference ability.

### 3.6. Determination of GSH in serum

To explore the feasibility of this method in the complex biological environment, this experiment was then applied to serum and we have made a labeled recovery experiment. Due to the high concentration of glutathione (GSH) in serum (mM level) [38] and the wide linear range of the system, the concentration of GSH in test system (1 mL) containing 100 μl serum was in the linear range of this experiment. Meanwhile, 30.0 μM, 50.0 μM and 80.0 μM GSH standard solution were added to the serum to perform the experiment. All data were based on three repeated measurements, as shown in Table 1. According to the standard curve (Fig. 5 (B)), the diluted concentration of GSH in serum was determined to be 46.0 μM corresponding serum original concentration is 0.460 mM which basically consistent with the content of GSH in serum [39]. The recoveries of GSH in serum were 95.0%, 98.5% and 96.6%, respectively (Table 1). In addition, the performance of the sensor for GSH detection was compared with previous analytical methods, and the results were summarized in Table 2. Compared with fluorescence and colorimetry, the detection limit of this work is close to or even lower, and the detection system designed by us has a wider linear range.

**Table 1**
Analytical results by this system for in real serum samples (n = 3).

| Samples | Found in sample (μM ± SD) | Added (μM) | Total found (μM ± SD) | Recovery rate (%) | RSD (%) |
|---|---|---|---|---|---|
| Serum | 46.0 ± 3.5 | 30.0 | 74.5 ± 1.6 | 95.0 | 5.5 |
| | | 50.0 | 95.3 ± 0.9 | 98.5 | 1.9 |
| | | 80.0 | 123.2 ± 2.4 | 96.6 | 3.2 |

## 4. Conclusion

In conclusion, we have successfully developed a glutathione (GSH) sensor based on chemiluminescence resonance energy transfer (CRET). According to the selective REDOX reaction between GSH and $MnO_2$NSs and the CRET between $FeS_2$NPs-Luminol and $MnO_2$NSs, a GSH turn-off-on sensor was established. In addition, the constructed sensor has good linearity in the range of 1–500 μM GSH, and good selectivity and sensitivity. The application of this system in the detection of GSH in serum is not only efficient, simple, but also has high specificity, which is expected to be applied to the detection of GSH in various environments.

**Table 2**
Comparison with previously reported methods for GSH detection.

| Materials | Materials | Linear range (μM) | LOD (μM) | Reference |
|---|---|---|---|---|
| Fluorescence | S-dots/ $Cu_2$ONP | 20–500 | 4 | [6] |
| Fluorescence | ZnS QDs | 2–104 | 0.9 | [40] |
| Colorimetry/ Photothermal analysis | $MnO_2$ nanosheets | 0.1–100/ 6.0–200 | 0.1/2 | [32] |
| Colorimetry | AA–Ag NPs | 5–50 | 0.24 | [7] |
| Chemiluminescence | $FeS_2$NPs/ $MnO_2$NSs | 1–500 | 0.15 | This work |

## Credit author contribution statement

Xiaomin Liu: Experiment design, Executed the experiment, Writing – original draft. Qian Fan, Xiaoxu Zhang: Executed the experiment. Ming Li, Yanfu Huan, Pinyi Ma, Daqiang Song: Writing – review & editing. Qiang Fei: Experiment design, Writing – review & editing.

## Declaration of competing interest

The authors declare that they have no known competing financial interests or personal relationships that could have appeared to influence the work reported in this paper.

## Acknowledgements

This work was supported by the Natural Science Foundation of Jilin Province, China (No. 20210101118JC).

## References

[1] P. Niu, Y. Rong, Y. Wang, H. Ni, M. Zhu, W. Chen, X. Liu, L. Wei, X. Song, A bifunctional fluorescent probe for simultaneous detection of GSH and H2Sn (n>1) from different channels with long-wavelength emission, Spectrochim. Acta Mol. Biomol. Spectrosc. 257 (2021) 119789.
[2] D. Fan, C. Shang, W. Gu, E. Wang, S. Dong, Introducing ratiometric fluorescence to MnO2 nanosheet-based biosensing: a simple, label-free ratiometric fluorescent sensor programmed by cascade logic circuit for ultrasensitive GSH detection, ACS Appl. Mater. Interfaces 9 (31) (2017) 25870–25877.
[3] T. Lorincz, A. Szarka, The determination of hepatic glutathione at tissue and subcellular level, J. Pharmacol. Toxicol. Methods 88 (2017) 32–39.
[4] M.D. Machado, E.V. Soares, Assessment of cellular reduced glutathione content in Pseudokirchneriella subcapitata using monochlorobimane, J. Appl. Phycol. 24 (6) (2012) 1509–1516.
[5] X. Wu, A. Shao, S. Zhu, Z. Guo, W. Zhu, A novel colorimetric and ratiometric NIR fluorescent sensor for glutathione based on dicyanomethylene-4H-pyran in living cells, Sci. China Chem. 59 (1) (2015) 62–69.
[6] S. Liu, J. Wang, Y.-e. Shi, Y. Zhai, Y.-k. Lv, P. Zhang, Z. Wang, Glutathione modulated fluorescence quenching of sulfur quantum dots by Cu2O nanoparticles for sensitive assay, Spectrochim. Acta Mol. Biomol. Spectrosc. 265 (2022).
[7] S.L. D'souza, R. Pati, S.K. Kailasa, Ascorbic acid-functionalized Ag NPs as a probe for colorimetric sensing of glutathione, Appl. Nanosci. 5 (6) (2014) 747–753.
[8] J. Yu, C. Li, S. Shen, X. Liu, Y. Peng, J. Zheng, Mass spectrometry based detection of glutathione with sensitivity for single-cell analysis, Rapid Commun. Mass Spectrom. 29 (7) (2015) 681–689.
[9] H. Xing, C. Peng, Y. Xue, Y. Fan, J. Li, E. Wang, In situ formed catalytic interface for boosting chemiluminescence, Anal. Chem. 92 (14) (2020) 10108–10113.
[10] F. Li, L. Guo, Z. Li, J. He, H. Cui, Temporal-spatial-color multiresolved chemiluminescence imaging for multiplex immunoassays using a smartphone coupled with microfluidic chip, Anal. Chem. 92 (10) (2020) 6827–6831.
[11] L. He, Z.W. Jiang, W. Li, C.M. Li, C.Z. Huang, Y.F. Li, In situ synthesis of gold nanoparticles/metal–organic gels hybrids with excellent peroxidase-like activity for sensitive chemiluminescence detection of organophosphorus pesticides, ACS Appl. Mater. Interfaces 10 (34) (2018) 28868–28876.
[12] F. Li, Y. Liu, M. Zhuang, H. Zhang, X. Liu, H. Cui, Biothiols as chelators for preparation of N-(aminobutyl)-N-(ethylisoluminol)/Cu2+ complexes bifunctionalized gold nanoparticles and sensitive sensing of pyrophosphate ion, ACS Appl. Mater. Interfaces 6 (20) (2014) 18104–18111.
[13] F. Luo, Y. Lin, L. Zheng, X. Lin, Y. Chi, Encapsulation of hemin in metal–organic frameworks for catalyzing the chemiluminescence reaction of the H2O2–luminol system and detecting glucose in the neutral condition, ACS Appl. Mater. Interfaces 7 (21) (2015) 11322–11329.
[14] D. Nagesh, S. Ghosh, A time period study on the efficiency of luminol in the detection of bloodstains concealed by paint on different surfaces, Forensic Sci. Int. 275 (2017) 1–7.
[15] Z.F. Zhang, H. Cui, C.Z. Lai, L.J. Liu, Gold nanoparticle-catalyzed luminol chemiluminescence and its analytical applications, Anal. Chem. 77 (2005) 3324–3329.
[16] S. Kanwal, Z. Traore, C. Zhao, X. Su, Enhancement effect of CdTe quantum dots–IgG bioconjugates on chemiluminescence of luminol–H2O2 system, J. Lumin. 130 (10) (2010) 1901–1906.
[17] F.J. Zheng, W. Ke, Y. Zhao, C.L. Xu, Pt NPs catalyzed chemiluminescence method for Hg2+ detection based on a flow injection system, Electrophoresis 40 (2019) 2218–2226.
[18] F. Zheng, W. Ke, Y. Zhao, C. Xu, Pt NPs catalyzed chemiluminescence method for Hg(2+) detection based on a flow injection system, Electrophoresis 40 (16–17) (2019) 2218–2226.
[19] Y.L. Cao, R. Yuan, Y.Q. Chai, L. Mao, H. Niu, H.J. Liu, Y. Zhuo, Ultrasensitive luminol electrochemiluminescence for protein detection based on in situ generated hydrogen peroxide as coreactant with glucose oxidase anchored AuNPs@MWCNTs labeling, Biosens. Bioelectron. 31 (1) (2012) 305–309.
[20] C.X. Wang, L.M. Chen, P.J. Wang, M.S. Li, D.F. Liu, A novel ultrasensitive electrochemiluminescence biosensor for glutathione detection based on poly-L-lysine as co-reactant and graphene-based poly(luminol/aniline) as nanoprobes, Biosens. Bioelectron. 133 (2019) 154–159.
[21] L. Hao, H. Gu, N. Duan, S. Wu, X. Ma, Y. Xia, Z. Tao, Z. Wang, An enhanced chemiluminescence resonance energy transfer aptasensor based on rolling circle amplification and WS2 nanosheet for Staphylococcus aureus detection, Anal. Chim. Acta 959 (2017) 83–90.
[22] X. Huang, L. Li, H. Qian, C. Dong, J. Ren, A resonance energy transfer between chemiluminescent donors and luminescent quantum-dots as acceptors (CRET), Angew Chem. Int. Ed. Engl. 45 (31) (2006) 5140–5143.
[23] Joon Seok Lee, Hyou-Arm Joung, Min-Gon Kim, C.B. Park, Graphene-based chemiluminescence resonance energy transfer for homogeneous immunoassay, ACS Nano 6 (2012) 2978–2983.
[24] H. Gao, W. Wang, Z. Wang, J. Han, Z. Fu, Amorphous carbon nanoparticle used as novel resonance energy transfer acceptor for chemiluminescent immunoassay of transferrin, Anal. Chim. Acta 819 (2014) 102–107.
[25] Y. Jia, X. Yi, Z. Li, L. Zhang, B. Yu, J. Zhang, X. Wang, X. Jia, Recent advance in biosensing applications based on two-dimensional transition metal oxide nanomaterials, Talanta 219 (2020) 121308.
[26] Y. Li, L.B. Zhang, Z. Zhang, Y. Liu, J. Chen, J. Liu, P.Y. Du, H.X. Guo, X.Q. Lu, MnO2 nanospheres assisted by cysteine combined with MnO2 nanosheets as a fluorescence resonance energy transfer system for "Switch-on" detection of glutathione, Anal. Chem. 93 (27) (2021) 9621–9627.
[27] Y.Y. Mi, X.X. Lei, H.Y. Han, J.G. Liang, L.Z. Liu, A sensitive label- free FRET probe for glutathione based on CdSe/ZnS quantum dots and MnO2 nanosheets, Anal. Methods 10 (34) (2018) 4170–4177.
[28] Y.H. Wang, K. Jiang, J.L. Zhu, L. Zhang, H.W. Lin, A FRET-based carbon dot-MnO2 nanosheet architecture for glutathione sensing in human whole blood samples, Chem. Commun. 51 (64) (2015) 12748–12751.
[29] X. Niu, Y. He, X. Li, H. Zhao, J. Pan, F. Qiu, M. Lan, A peroxidase-mimicking nanosensor with Hg2+-triggered enzymatic activity of cysteine-decorated ferromagnetic particles for ultrasensitive Hg2+ detection in environmental and biological fluids, Sensor. Actuator. B Chem. 281 (2019) 445–452.
[30] Z.Z. Dong, L. Lu, C.N. Ko, C. Yang, S. Li, M.Y. Lee, C.H. Leung, D.L. Ma, A MnO2 nanosheet-assisted GSH detection platform using an iridium(iii) complex as a switch-on luminescent probe, Nanoscale 9 (14) (2017) 4677–4682.
[31] T. Huang, S.N. Zhang, F. Huang, T.F. Gao, W.Y. Mao, Y.H. Wang, Infra-red spectroscopic study of Hongtoushan pyrite, Earth Sci. Front. 20 (2013) 104–109.
[32] D. Liu, Q. Tu, Y. Han, X. Wang, Q. Kang, P. Wang, W. Guo, A dual-modal colorimetric and photothermal assay for glutathione based on MnO2 nanosheets synthesized with eco-friendly materials, Anal. Bioanal. Chem. 412 (30) (2020) 8443–8450.
[33] C. Yao, J. Wang, A. Zheng, L. Wu, X. Zhang, X. Liu, A fluorescence sensing platform with the MnO2 nanosheets as an effective oxidant for glutathione detection, Sensor. Actuator. B Chem. 252 (2017) 30–36.
[34] S. Liu, M. Li, S. Li, H. Li, L. Yan, Synthesis and adsorption/photocatalysis performance of pyrite FeS2, Appl. Surf. Sci. 268 (2013) 213–217.
[35] A. Hung, I. Yarovsky, S.P. Russo, Density-functional theory studies of xanthate adsorption on the pyrite FeS2(110) and (111) surfaces, J. Chem. Phys. 118 (13) (2003) 6022–6029.
[36] W.S. Sun, W, Y.H. Hu, Yh, G.Q. Qiu, Gz, W.Q. Qin, Wq, Oxygen adsorption on pyrite (100) surface by density functional theory, J. Cent. S. Univ. Technol. 11 (2004) 385–390.
[37] C.-h. Zhao, J.-h. Chen, Y.-q. Li, Y. Chen, W.-z. Li, First-principle calculations of interaction of O2 with pyrite, marcasite and pyrrhotite surfaces, Trans. Nonferrous Metals Soc. China 26 (2) (2016) 519–526.
[38] Q.Y. Cai, J. Li, J. Ge, L. Zhang, Y.L. Hu, Z.H. Li, L.B. Qu, A rapid fluorescence "switch-on" assay for glutathione detection by using carbon dots-MnO2 nanocomposites, Biosens. Bioelectron. 72 (2015) 31–36.
[39] J. Xia, Z.W. Chen, M.M. Wu, C.Y. Ding, Determination of serum glutathione level and glutatione S-transferase activity in healthy college students, Chin. J. School Health 18 (1997) 273–274.
[40] Z. Amouzegar, A. Afkhami, T. Madrakian, ZnS quantum dots surface-loaded with zinc(II) ions as a viable fluorescent probe for glutathione, Mikrochim. Acta 186 (3) (2019) 205.